View metadata, citation and similar papers at core.ac.uk
brought to you by CORE
provided by Aston Publications Explorer

SNAP microresonators introduced by strong bending of optical fibers

Daria Bochek, Nikita Toropov, Ilya Vatnik, Dmitry Churkin, Misha Sumetsky

We introduce a new method of fabrication of Surface Nanoscale Axial Photonic (SNAP) microresonators by strong bending of an optical fiber. We experimentally demonstrate that geometric deformation and refractive index variation induced by bending is sufficient for the formation of a SNAP bottle resonator with nanoscale effective radius variation (ERV) along the fiber axis. In our experiment, we bend the optical fiber into a loop and investigate the properties of the fabricated tunable bottle resonator as a function of the loop dimensions. We find that the introduced ERV is approximately proportional to the local curvature of the loop while the ERV maximum is proportional to the maximum of the loop curvature squared. The advantages of the demonstrated method consist in its simplicity, robustness, and the ability of mechanical tuning of introduced resonant structures. This is of crucial importance for the creation of robust and tunable SNAP devices for applications in optical classical and quantum signal processing and ultraprecise sensing.

The high Q-factor optical microresonators have a great potential as basic elements of miniature signal processors and delay lines in optical communications [1-3], microlasers [1, 4, 5], ultraprecise sensors [4, 6], frequency comb generators [7], optomechanical devices [8], and quantum information devices [9, 10]. To date, two major platforms for the volume manufacturing of microresonator photonic devices have been developed: the ring resonator platform [2] and the photonic crystal platform [11]. The fabrication precision, low loss, and tunability of fabricated photonic circuits is being steadily improved. However, the achieved precision and loss level are still not sufficient for several practical applications such as fabrication of miniature optical delay lines and buffers [12, 13].

On the other hand, the Surface Nanoscale Axial Photonics (SNAP) platform [3, 14, 15], which utilizes whispering gallery mode (WGM) microresonators fabricated at the surfaces of optical fiber, combines the benefits of ultra-low loss and high fabrication precision. It was shown in [15, 16] that such a small variation of effective radius variation (ERV) is sufficient for strong localization of light and formation of microresonators and can be introduced with subangstrom precision. For example, the fabrication precision of SNAP was demonstrated to be better than 0.2 Å in ERV [15], which is almost two orders of magnitude better than that achieved in photonics technologies developed to date. In SNAP structures, WGMs circulate around the fiber surface while undergoing slow propagation along its axis. The axial propagation is fully controlled by the introduced nanoscale ERV of the optical fiber, which includes the contribution from the variations of refractive index and physical dimensions of the fiber.

Up to date two methods for creating of permanent SNAP resonators were demonstrated. The first method consists in local annealing of the fiber surface with a focused CO_2 laser beam which causes local thermal relaxation of the tension which was frozen-in during the fiber drawing [16]. The second method employs the femtosecond laser inscription which introduce local stresses inside the fiber [17]. Both methods allow to introduce nanoscale ERV of the optical fiber. Similar to the ring resonator and photonic crystal technologies, the future development of the SNAP platform will enable new important applications if SNAP structures are made tunable. While thermally tunable and fully reconfigurable SNAP microresonators have been demonstrated [18, 19], several applications (e.g., those in cavity quantum electrodynamics [20]) require or can benefit from their mechanical rather than thermal tuning.

In this Letter, we present a mechanically tunable SNAP platform which is based on effect of strong bending of an optical fiber on its ERV. Our approach can be applied to the uniform optical fibers as well as for tuning of SNAP structures fabricated by other methods described above. The setup used in our experiments is illustrated in Fig. 1.

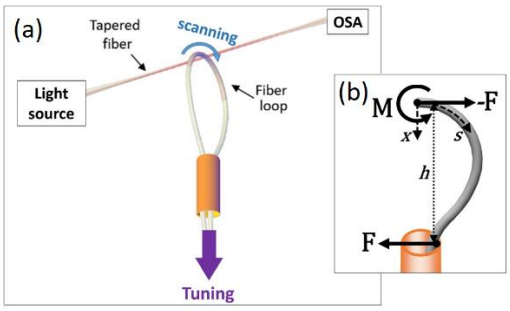

Fig. 1. (a) Illustration of experimental setup for the characterization of SNAP structure introduced by bending of an optical fiber. A micrometer diameter waist of a biconical tapered fiber (TF) is placed transversely to the bent optical fiber with a loop profile. The evanescent field in the waist of TF couples to WGMs which circulate inside the fiber loop due to the total internal reflection and undergo slow axial propagation controlled by the ERV of the fiber. The shape of the fiber loop is tuned by pulling/pushing the fiber ends. (b) The force pair $(\mathbf{F}, -\mathbf{F})$ and angular momentum $\mathbf{M}$ acting on the right half of the loop and keeping it in equilibrium.

The ends of the fiber, which was stripped from the coating and curved into a loop, were put through a narrow plastic tube. This simple setup allowed us to fix the loop shape as well as to tune it by pulling or pushing the fiber ends. Bending of the optical fiber causes its geometric deformation and, in particular, variation of its local effective radius r. In addition, bending introduces stresses which cause the variation of refractive index n due to the elasto-optic effect. In a series of experiments described below, we demonstrate that strong bending of the optical fiber results in the ERV which is sufficient for the formation of SNAP bottle resonators.

Slow propagation of WGMs along the axis s of the bent fiber is described by the one-dimensional wave equation [14]. In this equation, the wavenumber is expressed through the ERV $\Delta r_{eff}(s)$ and wavelength variation $\lambda - \lambda_c(s)$ where the WGM wavelength λ is assumed to be close to the cutoff wavelength $\lambda_c(s)$. Variation of $\lambda_c(s)$ can be rescaled to the ERV of the fiber:

$$\Delta\lambda_c(s) = \lambda_c \frac{\Delta r_{eff}(s)}{r_0}, \qquad (1)$$

where r_0 is the radius of the unbent optical fiber.

Experimentally, the WGM resonant spectrum is measured by a microfiber, specifically, a micron-diameter waist of a biconical tapered fiber (TF), which is fixed on a two-axis motorized translation stage and placed transversely to the test fiber axis, as illustrated in Fig. 1. The taper is connected to the light source and Optical Spectrum Analyzer (OSA) with switchable resolution of 1/0.04 pm and wavelength repeatability as high as +-3 pm. The SNAP structure is characterized by its spectrogram, i.e., the surface plot of resonant transmission spectra measured at series of equally spaced points along the microresonator axis. The spacing between these points determines the spatial resolution of measurements. An example of such spectrogram, which characterizes the ERV of the optical fiber introduced by bending to be discussed below is shown in Fig. 2(b).

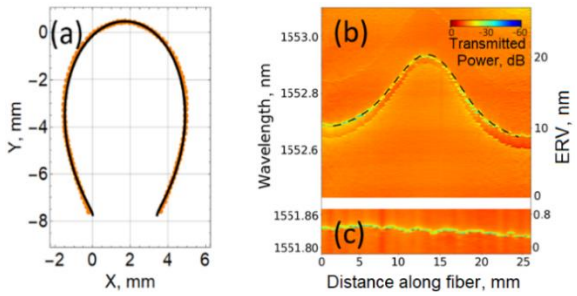

Fig. 2. Experimental characterization of the nanoscale ERV and spectrum of the bottle microresonator introduced by bending of the 125 μm optical fiber. (a) Measured profile of the fiber loop (red points) compared to its analytical approximation (black curve). (b) Spectrogram of the introduced SNAP bottle resonator measured with spatial resolution of 200 μm along the fiber axis. Black dashed curve is the rescaled curvature of the bent fiber. (c) Spectrogram of the same unbent fiber segment.

In our first experiment, we observed the ERV introduced by bending of a standard SMF-28 optical fiber. We found that the measured profile of the looped fiber used in this experiment (red points in Fig. 2(a)) is well approximated by the parametric curve (black line in Fig. 2(a)):

$$\begin{cases} x(t) = [(\sin(3t)\cdot a - b)\cdot\cos(t)]\cdot c - d \\ y(t) = [(\sin(3t)\cdot a - b)\cdot\sin(t)]\cdot f - g \end{cases}, \quad \textbf{(2)}$$

where constants $a = 0.48$ mm, $b = 0.7$ mm, $c = 9.15$ mm, $d = 1.71$ mm, $f = 7.8$ mm, and $g = 0.73$ mm were determined by fitting the experimental data. To determine the ERV of the bent fiber, we measured its spectrogram along the whole length of the loop with spatial resolution of 200 μm. In order to determine the actual ERV introduced by bending, we first characterized the ERV of the straight fiber.

The spectrograms of the SMF-28 fiber segment bent into a loop and of the same unbent segment are shown in Fig. 2(b) and (c), respectively. From Fig 2(c) and Eq. (1) we found that the straight optical fiber had an ERV with the slope of ~ 0.016 nm/mm. Comparison of Fig. 2(b) and (c) shows that, in this experiment, the original ERV of the unbent fiber was much smaller than the ERV of the introduced SNAP bottle resonator. In Fig. 2(b), there are two similar cutoff wavelength profiles which correspond to WGMs with different polarizations or different azimuthal and radial WGM quantum numbers. Considering for determinacy the more contrast upper profile, we found that the introduced maximum ERV $\Delta r_{eff}^{(max)}$ at the top of the fiber loop is related to the maximum cutoff wavelength variation $\Delta\lambda_c^{(max)}$ by the rescaling relation, of Eq. (1) where the cutoff wavelength found from Fig. 2(b) is $\lambda_c = 1552.7$ nm. From this relation, the observed maximum wavelength variation $\Delta\lambda_c^{(max)} = 0.25$ nm (Fig. 2(b)) corresponds to the ERV $\Delta r_{eff}^{(max)} = 10.1$ nm. Using Eq. (2) we determined the curvature of the loop along the axis of the fiber. The rescaled curvature variation is presented by a black dashed curve in Fig. 2(b).

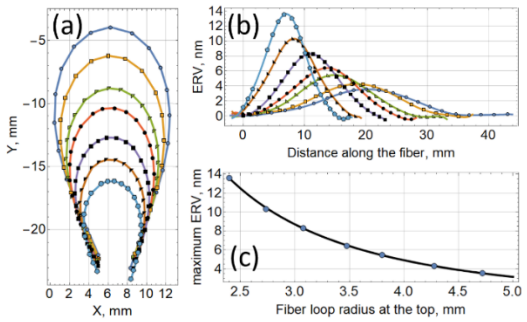

Fig. 3. (a) Profiles of optical fiber loops investigated. (b) Measured ERV distributions along the loops where the curve with largest ERV corresponds to the smallest loop in (a). (c) The maximum ERV at the top point of the loop versus its radius at the same point. Black curve is approximation of experimental data with $\Delta r_{eff}^{(max)} = 0.28 r_0^3 / R_0^2$.

Comparison of this curve with the ERV profile shows that, with a good accuracy, the ERV of bent optical fiber is proportional to the local curvature of the loop. The measured value of Q-factor of the resonator is ~10^6 and does not depend on the fiber curvature.

In our second experiment, we investigated the SNAP bottle resonators introduced by seven fiber loops with different sizes shown in Fig. 3(a). We measured the spectrograms of these loops (similar to that shown in Fig. 2(b)) starting with the biggest loop (dark blue curve), the size of which was reduced down to the smallest loop (light blue curve) by pulling the ends of the fiber as illustrated in Fig. 1. The ERV curves found from the spectrograms are shown in Fig. 3(b) and have the same colors as the corresponding fiber loops in Fig. 3(a). The maximum ERV values, which corresponds to the top of the loops, are plotted in Fig 3(c) as a function of the loop radius R_0 at its top. Fitting the experimental results allowed us to come up with the empirical relation between the ERV and local curvature radius $R(s)$ of the fiber:

$$\Delta r_{eff}(s) = 0.28 r_0^3 / (R_0 R(s)), \quad \textbf{(3)}$$

where R_0 is loop radius at its top, which axial coordinate we set to $s = 0$ so that $R_0 = R(0)$. The equation indicates on the quadratic dependence of the maximum relative ERV $\Delta r_{eff}^{(max)} / r_0$ on r_0 / R_0 and linear dependence of $\Delta r_{eff}(s)$ on local curvature of the fiber.

In our third experiment, to arrive at smaller dimensions of the SNAP bottle resonator and to investigate the dependence of the discovered effect on the fiber radius, we introduced it using an optical fiber with radius $r_0 = 20$ μm. The standard SMF-28 fiber cannot be curved into a loop with less than ~ 3-4 mm dimensions because of the strength limit. However, a 20 μm radius fiber can be bent into a loop with sub-millimeter dimensions. The profile of the loop, which was fabricated using the approach illustrated in Fig. 1, is shown by red points in Fig. 4(a) and approximated by black parametric curve determined by Eq. (2) with constants $a = 9.7$ mm, $b = 0.16$ mm, $c = 9.15$ mm, $d = 0.46$ mm, $f = 7.66$ mm, and $g = 0.28$ mm. The spectrogram of this loop and of the same straight section are shown in Fig. 4(b, c). It is seen from Fig. 4(c) that the original ERV of the straight fiber was significantly greater than that for the SMF-28 fiber characterized in Fig. 2(c). Therefore, in order to compare the ERV profile introduced by bending with the distribution of the local loop curvature (similar to the comparison shown in Fig. 2(b) for the SMF-28 fiber), we took this original ERV into account. Specifically, the dashed black curve in Fig. 4(b) shows the rescaled loop curvature profile plus the original linear ERV of the fiber found from Fig. 4(c). Similar to the case of the SMF-28, we observed that the dependence of the ERV introduced by bending was proportional to the local loop curvature. Note that the relatively large original linear ERV of this fiber does not affect the parabolic shape of the introduced microresonator which is important for several applications [3].

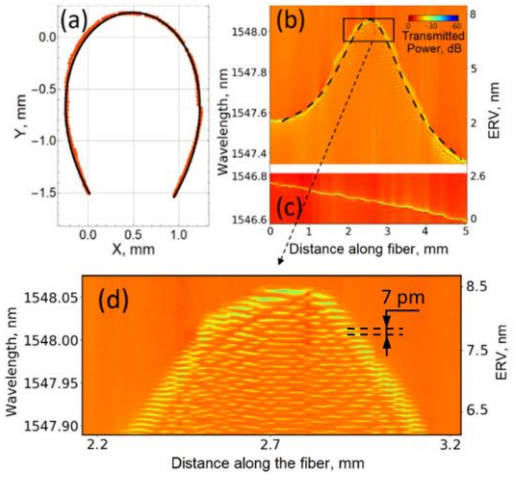

Fig. 4. Investigation of the SNAP bottle resonator introduced by bending of the 20 μm radius optical fiber. (a) Measured profile of the optical fiber loop (red points). Black solid curve is the fit of the measured loop profile with parametric Eq. (2). (b) The spectrogram measured with spatial resolution of 35 μm along the fiber loop shown in (a). Black dashed curve represents the sum of the rescaled local curvature distribution of the bent fiber and the original linear ERV of the same fiber segment. (c) Spectrogram of the same unbent fiber segment. (d) Magnified region of the spectrogram outlined in (b) that resolves axial modes near the top of the introduced bottle resonator.

Remarkably, the axial size of the resonator formed by the 20 □m radius fiber is noticeably smaller than that formed by the SMF-28 fiber while its ERV is of the same order. The localized axial modes of this resonator can be resolved by magnifying the region outlined by a black rectangle in Fig. 4(b), which is shown in Fig. 4(d). The observed discrete spectrum confirms the existence of WGMs localized within the millimeter-scale length of the created SNAP bottle resonator. We determined the free spectral range of these modes in the vicinity of the top of the loop by approximating the measured ERV by the parabolic dependence $\Delta r_{eff}(s) = -s^2/(2R_0)$ with axial radius $R_0 \approx 70$ m. In this approximation, the free spectral range of the axial resonances is determined from the equation [23]:

$$\Delta\lambda_{FSR} = \lambda_c^2 (2\pi n)^{-1} (r_0 R_0)^{-1/2}. \quad \textbf{(4)}$$

For the silica fiber with refractive index $n = 1.46$ and radius $r_0 = 20$ μm at the cutoff wavelength $\lambda_c = 1.55$ μm, we have $\Delta\lambda_{FSR} = 7$ pm in good agreement with the experimental data shown in Fig. 4(d).

In the preliminary analysis of experimental results obtained, we considered a model shown in the Fig. 1(b) replicating the behavior of the fiber loop of our experiment. In this model, the right-hand side of the fiber loop is fixed at its axial coordinate $s = 0$ and the force $\mathbf{F}$ applied to the loop determines the reaction of the tube. Since the fiber segment shown in this figure is in equilibrium, the value of the angular momentum $\mathbf{M}$ applied at the cross-section $s = 0$ from the left-hand side part of the loop (not shown) should be equal to hF where h is the arm of the couple $(\mathbf{F}, -\mathbf{F})$, $F = |\mathbf{F}|$, and $M = |\mathbf{M}|$. For small s, near the top of the loop, the deformations u_x, u_y, and u_z of the fiber along the x, y, and z directions is described in the linear approximation in r_0 / R_0 as [24]

$$u_x = \frac{M}{2EI}\left[z^2 + \nu(x^2 - y^2)\right] - \frac{F}{EA}x, \quad \textbf{(5)}$$

$$u_y = \frac{M}{EI}\nu xy - \frac{F}{EA}y, \quad u_z = \frac{F}{EA}z, \quad \textbf{(6)}$$

Here $I = \pi r_0^4 / 4$ is the bending moment of inertia of the fiber, $A = \pi r_0^2$ is its cross-section area, $E = 7 \cdot 10^9$ Pa, is the Young's modulus, $\nu = 0.17$ is the Poisson ratio, and y and z are the coordinates normal to

x oriented normal and parallel to the plane of the picture, respectively. From Eq. (5), the fiber curvature at $s = 0$ is $1/R_0 = d^2u_x/ds^2 = M/EI$. From this equation, the fiber curvature radius $R_0 = 2.1$ mm and arm $h = 10$ mm of the 62.5 μm radius fiber loop shown in Fig. 2(a) correspond to $F = 0.08$ N and $M = 8 \cdot 10^{-3}$ N·m. It is seen from Eqs. (5) and (6) that the terms proportional to M are antisymmetric in x and y. Therefore, their contribution into the ERV, which is calculated by averaging over the azimuthal angle in the fiber cross-section [16], vanishes. The remaining terms being proportional to F result in variation of the fiber radius by $\Delta r = \nu F r_0 / EA$; 1 nm and variation of the refractive index by $\Delta n = C_2 F / A$; $2.6 \cdot 10^{-5}$ which corresponds to the ERV $\Delta n r_0 / n$; 1 nm (here $C_2 = 4 \cdot 10^{-12}$ Pa^{-1} is the stress-optic coefficient of silica [25]). Both values are significantly smaller than those observed experimentally (see Fig. 2(b)). Therefore, we suggest that the major contribution to the observed ERV is given by the nonlinear terms $\sim r_0^2 / R_0^2$ neglected in Eqs. (5) and (6). In particular, for the fiber with radius $r_0 = 62.5$ μm these terms may contribute to the ERV as much as $u_x r_0 / R_0 \sim \nu r_0^3 / R_0^2$; 10 nm, which is comparable with the ERV observed experimentally.

In conclusion, we have demonstrated a new technique for fabrication of tunable SNAP microresonators at the surface of a silica fiber. Our approach is much simpler than those developed previously, since it does not require the use of lasers and consists only in controllable fiber bending. The theoretical description of the observed elasto-optical effects leading to the formation of SNAP bottle resonators, and in particular, accurate calculation of the ERV along the bent fiber requires the numerical solution of the nonlinear equations of elasticity is underway and will be reported elsewhere. The proposed experimental setup used is simple and therefore enables fabrication of simplest tunable SNAP bottle resonators. The ability to tune the introduced resonant structures mechanically is of great importance for the creation of robust and tunable SNAP devices which can be used for applications in classical and quantum optical signal processing as well as ultraprecise sensing.

References

1. A. B. Matsko (Ed), Practical Applications of Microresonators in Optics and Photonics, (CRC Press, 2009).
2. W. Bogaerts, P. De Heyn, T. Van Vaerenbergh, K. De Vos, S. K. Selvaraja, T. Claes, P. Dumon, P. Bienstman, D. Van Thourhout, and R. Baets, Laser Photonics Rev. **6**, 47 (2012).
3. M. Sumetsky, Phys. Rev. Lett. **111**, 163901 (2013).
4. T. Reynolds, N. Riesen, A. Meldrum, X. D. Fan, J. M. M. Hall, T. M. Monro, and A. François, Laser Photonics Rev. **11**, 1600265 (2017).
5. M. Sumetsky, Light: Sci. & Appl. 6, e17102 (2017).
6. M. R. Foreman, J. D. Swaim, and Frank Vollmer, Adv. Opt. Photon. **7**, 168 (2015).
7. T. J. Kippenberg, R. Holzwarth, and S. A. Diddams, Science 332, 555 (2011).
8. M. Aspelmeyer, T. J. Kippenberg, and F. Marquardt, Rev. Mod. Phys. **86**, 1391 (2014).
9. H. J. Kimble, Nature **453**, 1023 (2008).
10. A. Reiserer and G. Rempe,"Cavity-based quantum networks with single atoms and optical photons," Rev. Mod. Phys. **87**, 1379 (2015).
11. M. Notomi, E. Kuramochi, and T. Tanabe, Nature Photon. **2**, 741 (2008).
12. E. F. Burmeister, D. J. Blumenthal, and J. E. Bowers, Opt. Switch. Netw. **5**, 10 (2008).
13. W. Bogaerts, M. Fiers, and P. Dumon, IEEE J. Sel. Top. Quantum Electron. **20**, 1 (2014).
14. M. Sumetsky, D. J. DiGiovanni, Y. Dulashko, J. M. Fini, X. Liu, E. M. Monberg, and T. F. Taunay, Opt. Lett. **36**, 4824 (2011).
15. M. Sumetsky, Opt. Express **20**, 22537 (2012).
16. N. A. Toropov and M. Sumetsky, Opt. Lett. **41**, 2278 (2016).
17. F. C. Shen, X. W. Shu, L. Zhang, and M. Sumetsky, Opt. Lett. **41**, 2795 (2016).
18. A. Dmitriev, N. Toropov, and M. Sumetsky, IEEE Photonics Conference (IPC), 2015, Postdeadline paper, p.1.

19. D. L. P. Vitullo, S. Zaki, G. Gardosi, B. J. Mangan, R. S. Windeler, M. Brodsky, and M. Sumetsky, Opt. Lett. **43**, 4316 (2018).
20. M. Pöllinger, D. O'Shea, F. Warken, and A. Rauschenbeutel, Phys. Rev. Lett. **103**, 053901 (2009).
21. N. I. Muskhelishvili, *Some Basic Problems of the Mathematical Theory of Elasticity*, Springer Science & Business Media, 2013.
22. T. A. Birks, J.C. Knight, and T. E. Dimmick, Phot. Technol. Lett. **12**, 182 (2000).
23. M. Sumetsky and Y. Dulashko, Opt. Lett. **35**, 4006 (2010).
24. M. Sumetsky and J. M. Fini, Opt. Express **19**, 26470 (2011).
25. W. Primak and D. Post, J. Appl. Phys. **30**, 779 (1959).

References with titles

1. A. B. Matsko (Ed), Practical Applications of Microresonators in Optics and Photonics, (CRC Press, 2009).
2. W. Bogaerts, P. De Heyn, T. Van Vaerenbergh, K. De Vos, S. K. Selvaraja, T. Claes, P. Dumon, P. Bienstman, D. Van Thourhout, and R. Baets, "Silicon microring resonators," Laser Photonics Rev. 6, 47 (2012).
3. M. Sumetsky, "Delay of light in an optical bottle resonator with nanoscale radius variation: dispersionless, broadband, and low loss", Phys. Rev. Lett. 111, 163901 (2013).
4. T. Reynolds, N. Riesen, A. Meldrum, X. D. Fan, J. M. M. Hall, T. M. Monro, and A. François, "Fluorescent and lasing whispering gallery mode microresonators for sensing applications," Laser Photonics Rev. 11, 1600265 (2017).
5. M. Sumetsky, "Lasing microbottles," Light: Sci. & Appl. 6, e17102 (2017).
6. M. R. Foreman, J. D. Swaim, and Frank Vollmer, "Whispering gallery mode sensors," Adv. Opt. Photon. 7, 168 (2015).
7. T. J. Kippenberg, R. Holzwarth, and S. A. Diddams, "Microresonator-based optical frequency combs," Science 332, 555 (2011).
8. M. Aspelmeyer, T. J. Kippenberg, and F. Marquardt, "Cavity optomechanics," Rev. Mod. Phys. 86, 1391 (2014).
9. H. J. Kimble, "The quantum internet," Nature 453, 1023 (2008).
10. A. Reiserer and G. Rempe,"Cavity-based quantum networks with single atoms and optical photons," Rev. Mod. Phys. 87, 1379 (2015).
11. M. Notomi, E. Kuramochi, and T. Tanabe, "Large-scale arrays of ultrahigh-Q coupled nanocavities," Nature Photon. 2, 741 (2008).
12. E. F. Burmeister, D. J. Blumenthal, and J. E. Bowers, "A comparison of optical buffering technologies," Opt. Switch. Netw. 5, 10 (2008).
13. W. Bogaerts, M. Fiers, and P. Dumon, "Design Challenges in Silicon Photonics," IEEE J. Sel. Top. Quantum Electron. 20, 1 (2014).
14. M. Sumetsky, D. J. DiGiovanni, Y. Dulashko, J. M. Fini, X. Liu, E. M. Monberg, and T. F. Taunay, "Surface nanoscale axial photonics: robust fabrication of high-quality-factor microresonators," Opt. Lett. 36, 4824 (2011).
15. M. Sumetsky, "Theory of SNAP devices: basic equations and comparison with the experiment," Opt. Express 20, 22537 (2012).
16. N. A. Toropov and M. Sumetsky, "Permanent matching of coupled optical bottle resonators with better than 0.16 GHz precision," Opt. Lett. 41, 2278 (2016).
17. F. C. Shen, X. W. Shu, L. Zhang, and M. Sumetsky, "Fabrication of surface nanoscale axial photonics structures with a femtosecond laser," Opt. Lett. 41, 2795 (2016).
18. A. Dmitriev, N. Toropov, and M. Sumetsky, "Transient reconfigurable subangstrom-precise photonic circuits at the optical fiber surface," IEEE Photonics Conference (IPC), 2015, Postdeadline paper, p.1.
19. D. L. P. Vitullo, S. Zaki, G. Gardosi, B. J. Mangan, R. S. Windeler, M. Brodsky, and M. Sumetsky, "Tunable SNAP microresonators via internal ohmic heating," Opt. Lett. 43, 4316 (2018).
20. M. Pöllinger, D. O'Shea, F. Warken, and A. Rauschenbeutel, "Ultrahigh-Tunable Whispering-Gallery-Mode Microresonator," Phys. Rev. Lett. 103, 053901 (2009).
21. N. I. Muskhelishvili, *Some Basic Problems of the Mathematical Theory of Elasticity*, Springer Science & Business Media, 2013.
22. T. A. Birks, J.C. Knight, and T. E. Dimmick, "High-resolution measurement of the fiber diameter variations using whispering gallery modes and no optical alignment," Phot. Technol. Lett. 12, 182 (2000).

23. M. Sumetsky and Y. Dulashko, "Radius variation of optical fibers with angstrom accuracy," Opt. Lett. 35, 4006 (2010).
24. M. Sumetsky and J. M. Fini, "Surface Nanoscale Axial Photonics," Opt. Express 19, 26470 (2011).
25. W. Primak and D. Post, "Photoelastic constants of vitreous silica and its elastic coefficient of refractive index," J. Appl. Phys. 30, 779 (1959).